Published in final edited form as:
Vis Neurosci. 2008 ; 25(5-6): 693–700.

Light regulation of Ca^{2+} in the cone photoreceptor synaptic terminal

Sue-Yeon Choi[1], **Skyler Jackman**[2], **Wallace B. Thoreson**[3], and **Richard H. Kramer**[1]

[1]Department of Molecular and Cell Biology, University of California, Berkeley, California

[2]Department of Physics, University of California, Berkeley, California

[3]Department of Ophthalmology and Visual Sciences, University of Nebraska Medical Center, Omaha, Nebraska

Abstract

Retinal cones are depolarized in darkness, keeping voltage-gated Ca^{2+} channels open and sustaining exocytosis of synaptic vesicles. Light hyperpolarizes the membrane potential, closing Ca^{2+} channels and suppressing exocytosis. Here, we quantify the Ca^{2+} concentration in cone terminals, with Ca^{2+} indicator dyes. Two-photon ratiometric imaging of fura-2 shows that global Ca^{2+} averages ~360 nM in darkness and falls to ~190 nM in bright light. Depolarizing cones from their light to their dark membrane potential reveals hot spots of Ca^{2+} that co-label with a fluorescent probe for the synaptic ribbon protein ribeye, consistent with tight localization of Ca^{2+} channels near ribbons. Measurements with a low-affinity Ca^{2+} indicator show that the local Ca^{2+} concentration near the ribbon exceeds 4 μM in darkness. The high level of Ca^{2+} near the ribbon combined with previous estimates of the Ca^{2+} sensitivity of release leads to a predicted dark release rate that is much faster than observed, suggesting that the cone synapse operates in a maintained state of synaptic depression in darkness.

Keywords

Cone; Photoreceptor; Ca^{2+}; Synaptic transmission; Exocytosis

Introduction

The biochemical signaling steps of rod and cone phototransduction are known in quantitative detail, but our understanding of how the light response is transmitted to postsynaptic neurons is more limited. We know that sustained depolarization in darkness activates L-type Ca^{2+} channels in photoreceptor terminals (Corey et al., 1984; Wilkinson & Barnes, 1996; Baldridge et al., 1998) and that intracellular Ca^{2+} is required for synaptic vesicle exocytosis, which occurs tonically in darkness (Cervetto & Piccolino, 1974). Intraterminal Ca^{2+} is known to decrease in the light (Johnson et al., 2007), but the concentrations of Ca^{2+} that underlie synaptic vesicle release in darkness and light have not been accurately quantified with ratiometric Ca^{2+} indicators.

Previous studies on isolated photoreceptors (Rieke & Schwartz, 1996) provided estimates of Ca^{2+} in terminals by using voltage clamp to hold the membrane potential near the expected dark and light voltages. In cone terminals, the steady-state Ca^{2+} concentration is a consequence of influx through ion channels [both L-type Ca^{2+} channels and cyclic nucleotide-gated (CNG)

Address correspondence to: Richard H. Kramer, Department of Molecular and Cell Biology, University of California, 121 Life Sciences Addition, Berkeley, CA 94720-3200. rhkramer@berkeley.edu.

channels; Savchenko et al., 1997], balanced by cytoplasmic buffering and efflux through the plasma membrane Ca^{2+}-ATPase (Morgans et al., 1998; Krizaj & Copenhagen, 1998). In rods, Ca^{2+}-dependent Ca^{2+} release from intracellular stores also plays a role in setting the intracellular Ca^{2+} level (Krizaj et al., 1999, 2003; Cadetti et al., 2006; Suryanarayanan & Slaughter, 2006). We have shown previously that the dark Ca^{2+} concentration is maintained at a lower concentration in rods than in cones, accounting for the slower dark rate of exocytosis in rods than in cones (Sheng et al., 2007).

Here, we measure Ca^{2+} in cone synaptic terminals with the fluorescent ratiometric indicator dye, fura-2. To monitor Ca^{2+} in darkness, we use two-photon microscopy, in which infrared light excites dye fluorescence in cone terminals while minimally exciting phototransduction in outer segments. Infrared light penetrates deeply into tissue, enabling visualization of Ca^{2+} in cone terminals in the intact retina. To localize subcellular sites of Ca^{2+} entry, we examine individual cone terminals more closely in retinal slices with low-affinity nonratiometric Ca^{2+} dyes dialyzed into cells with a patch pipette.

Photoreceptor terminals have synaptic ribbons which play a role in tonic release, but the specific function of the ribbon is unclear (Prescott & Zenisek, 2005). Voltage-gated Ca^{2+} channels are found adjacent to ribbons (Nachman-Clewner et al., 1999; Morgans, 2001), consistent with local control of Ca^{2+}-dependent exocytosis at the plasma membrane, but other Ca^{2+}-dependent events may also occur at the ribbon (Heidelberger et al., 2005). Measuring and localizing light-induced changes in the Ca^{2+} concentration will help constrain the possible locations and affinities of Ca^{2+} sensors for vesicle replenishment and exocytosis, bringing us closer to understanding how neurotransmission is regulated at the ribbon synapse.

Materials and methods

Tissue preparation and dye loading

The retina from the lizard, *Anolis segrei*, was isolated with the retinal pigment epithelium attached (Choi et al., 2005a,b; Sheng et al., 2007) with procedures approved by the UC Berkeley Animal Care and Use Committee. The retina was prepared and imaged in saline containing (in mM) NaCl 149, KCl 4, $CaCl_2$ 1.5, $MgCl_2$ 1.5, HEPES 10, Glucose 10 (pH 7.4). First, a membrane-permeant Ca^{2+} indicator dye, either Oregon Green BAPTA-1-AM (OGB-1) or fura-2-AM, was applied at 100 μM for 2 h to load retinal cells. The saline contained 1% DMSO and 0.2% pluronic acid to enhance dye solubility and cell permeation. Dye-loaded retinas were then mounted flat on nitrocellulose filter paper with the inner retina facing the microscope objective. For dual imaging of synaptic vesicles and Ca^{2+}, the retina was double labeled, first with FM 4-64 (Choi et al., 2005a) and then with fura-2-AM. Retinal preparation and labeling were carried out at 21°C in complete darkness.

The retina from the larval tiger salamander, *Ambystoma tigrinum*, was isolated with procedures approved by the University of Nebraska Medical Center Institutional Animal Care and Use Committee. Retinal slices were prepared (Rabl et al., 2005), and whole-cell voltage-clamp recordings were obtained with an Optopatch patch-clamp amplifier (Cairn Instruments, Faversham, Kent, UK) with 8–15 Mohm borosilicate glass patch electrodes. The pipette solution contained (in mM) 94 CsGluconate, 9.4 TEACl, 1.9 $MgCl_2$, 9.4 MgATP, 0.5 GTP, 0.5 EGTA, 32.9 HEPES (pH 7.2). To label the synaptic ribbon, a rhodamine-conjugated ribeye peptide (Zenisek et al., 2004) was used at 50 μM.

Imaging

Anole cones were imaged with a Zeiss LSM two-photon microscope equipped with a tunable Mai-Tai laser (Spectraphysics, Mountain view, CA). The excitation wavelength was tuned to

800 nm for OGB-1 and 700 and 760 nm for ratiometric imaging of fura-2. To stimulate cone phototransduction, we used white light from a halogen lamp with intensity of 10^7 photons/μm^2/s, attenuated with neutral density filters. Images were analyzed with Scion Image software (Scion Corporation, Frederick, MD).

The intraterminal Ca^{2+} concentration of anole cones was calculated from the ratio of emitted light evoked by two-photon dye excitation of fura-2 with 700- and 760-nm light, with standard equations (Grynkiewicz et al., 1985). Calibration constants were determined using a fura-2 calcium imaging calibration kit (Invitrogen) as described previously (Sheng et al., 2007), yielding a K_d of 234 nM (Fig. 1G). A similar midpoint ratio value was obtained *in situ* by recording from individual lizard cones and dialyzing them with highly buffered, known concentrations of Ca^{2+}. For the midpoint ratio, the pipette solution had a free Ca^{2+} concentration of 180 nM and consisted of (in mM) 132 KCl, 2 NaCl, 10 EGTA, 3.5 $CaCl_2$, 2 $MgCl_2$, 20 HEPES (pH 7.1, $N = 8$ cells). The minimum and maximum ratios were obtained by dialyzing solutions containing 0 $CaCl_2$ ($N = 4$) or 0 EGTA ($N = 6$).

Salamander cones were imaged with a spinning disk confocal microscope (Perkin Elmer Ultraview LCI) equipped with a cooled CCD camera (Orca ER, Hama-matsu Corp., Japan). Images were acquired at 60-ms intervals with single-frame durations of 48–56 ms. Pixel values were binned 2 × 2. Ca^{2+} indicator dyes were included in the patch pipette at 100 μM and were dialyzed into cells during whole-cell recording. We used three dyes: Oregon Green BAPTA-1 (OGB), Oregon Green BAPTA-6F (OGB-6F), and Oregon Green 488 BAPTA-5N (OGB-5N), with K_d values of 0.17, 3, and 20 μM, respectively, as reported by Molecular Probes (Eugene, OR). We estimated changes in Ca^{2+} with OGB-5N by using the following equation (Helmchen, 2000):

$$\Delta[Ca^{2+}]_i = \left(\left[Ca^{2+}\right]_{\text{rest}} + K_d\,(\Delta F/F)\,/(\Delta F/F)_{\max}\right) / \left(1 - (\Delta F/F)\,/(\Delta F/F)_{\max}\right). \quad (1)$$

$\Delta F/F$ represents the fractional change in fluorescence resulting from a brief depolarizing step. $(\Delta F/F)_{\max}$ was determined from the maximal fluorescence change produced by a 500-ms depolarization to −10 mV. Variability in the amount of dye that enters each cell during whole-cell recording produces cell-to-cell differences in absolute fluorescence that prevented *in situ* determination of the K_d for OGB-5N. We therefore used the K_d value of 20 μM provided by Molecular Probes. There was no added Ca^{2+} in the pipette solution, and thus, the resting Ca^{2+} concentration ($[Ca^{2+}]_{\text{rest}}$) was assumed to be 10 nM, but varying this value from 1 to 100 nM had only a small effect (<100 nM) on the calculated value of $\Delta[Ca^{2+}]_i$. To validate measurements obtained using eqn (1), we measured fluorescence changes produced by the three different Oregon Green dyes under identical stimulation conditions and obtained similar estimates of intraterminal Ca^{2+} concentration. This comparison was carried out in salamander rods because recordings are more stable and fluorescent hot spots larger and easier to measure than in cones (unpublished observations).

Results

Illumination causes a decrease in the cone terminal Ca^{2+} concentration

We first examined light-regulated changes in synaptic Ca^{2+} in flat mounts of the cone-only retina of the anole lizard. Cone terminals in the outer plexiform layer (OPL) were identified by their loading with the synaptic vesicle marker dye FM4-64 (Rea et al., 2004). The same terminals also label strongly with the nonratiometric Ca^{2+} indicator Oregon Green BAPTA-1 (OGB) (Fig. 1A). Light stimulation results in a decrease in dye fluorescence, indicating a drop

in intraterminal Ca^{2+} concentration (Fig. 1B). A difference image from scans of the OPL before and after exposure to white light reveals a decrease in Ca^{2+} in nearly all the cone terminals (Fig. 1C). We controlled for possible effects of the laser scan by constructing a difference image from repeated scans in the dark. Repeated scanning alone caused no change in Ca^{2+} (Fig. 1D–1F).

To quantify the change in Ca^{2+} elicited by light stimulation, we used the ratiometric Ca^{2+} indicator fura-2. Scans of the OPL were obtained with 700- and 760-nm light to minimize photostimulation of cones, and pixel-by-pixel ratio values were converted into Ca^{2+} concentrations. To enable this conversion, we calibrated the Ca^{2+} dependence of the 700:760 nm fura-2 excitation ratio in test solutions (Fig. 1G). A complete *in situ* dye calibration in patch-clamped cones was not possible because high Ca^{2+} concentrations resulted in cell death. However, we did confirm that dialysis into cones of a solution containing 180 nM free Ca^{2+} produced an excitation ratio of 1.32 ± 0.04 (n = 8), in good agreement with the ratio predicted from the cell-free calibration (1.31). These measurements indicate that the average Ca^{2+} concentration in cone terminals was ~359 ± 24 nM in darkness (n = 8) but dropped to ~188 ± 10 nM after a 5-min exposure to bright white light (n = 8) (Fig. 1H). We observed that the decrease in Ca^{2+} elicited by light was slow to develop (>2 min), presumably resulting from slow-buffered diffusion of Ca^{2+} throughout the cytoplasm of the cone terminal. Hence, the steady-state concentration of Ca^{2+} in bright light is likely to be underestimated. Consistent with the notion that prolonged cessation of Ca^{2+} entry would lower Ca^{2+} further, application of Ca^{2+}-free saline for 15 min resulted in a larger decrease in internal Ca^{2+} to ~88 ± 7 nM (n = 4).

To investigate the role of phototransduction in mediating the effect of light on intraterminal Ca^{2+}, we applied the phosphodiesterase (PDE) inhibitor isobutylmethylxanthine (IBMX). We found that IBMX eliminated the light-dark difference and also elevated the basal Ca^{2+} concentration to ~450 nM. IBMX inhibition of PDE leads to a supranormal accumulation of cGMP, thereby opening CNG channels in cone terminals (Savchenko et al., 1997) and outer segments (Fesenko et al., 1985). Enhancement of the CNG current can lead to membrane depolarization and greater Ca^{2+} influx, which could contribute to elevating basal Ca^{2+} and blunting the light-dark difference in synaptic Ca^{2+} concentration.

Ca^{2+} entry is localized to synaptic ribbons

To localize sites of Ca^{2+} entry in cone terminals, we imaged Ca^{2+} changes resulting from depolarizing steps. Ca^{2+} indicator dyes were introduced through an inner segment-attached patch electrode. A long axon separates the terminal from the inner segment of anole cones, so to avoid possible space clamp errors, we used tiger salamander cones, which have a synaptic terminal incorporated directly into the inner segment.

The Ca^{2+} concentration in the nm-scale region (the "nanodomain") adjacent to the inner mouth of an open Ca^{2+} channel is likely to exceed 100 μM (Matthews, 1996; Naraghi & Neher, 1997; Demuro & Parker, 2006). Consistent with this, we found that activating the Ca^{2+} current by applying depolarizing steps from −70 to −10 mV produced a localized change in Ca^{2+} that could be visualized with the low-affinity Ca^{2+} dye, OGB-5N, which has a K_d of 20 μM. Subtraction of the image obtained at −70 mV (Fig. 2A1) from that obtained at −10 mV (Fig. 2A2) yields a difference image (Fig. 2A3), revealing a "hot spot" of Ca^{2+} in the synaptic terminal region at the base of the cone. We converted fluorescence changes in a 2-μm^2 region at the center of the hot spot into Ca^{2+} levels with eqn (1) (see Methods), yielding an estimate of 8.1 ± 1.1 μM (N = 6). For the experiment in Fig. 2, we plotted Ca^{2+} changes as a function of time. The graph at the left shows Ca^{2+} levels measured in the hot spot, and the graph at the right shows Ca^{2+} levels measured in an adjacent region (just to the upper right of the hot spot) and a region in the center of the soma. The graph shows that Ca^{2+} levels rise abruptly during

the test step and fall quickly afterward. Because diffraction limits of light microscopy blur accurate localization of fluorescence, these measurements underestimate the Ca^{2+} concentration adjacent to the open pore of a voltage-gated Ca^{2+} channel. Unlike what is found in rods (Cadetti et al., 2006; Suryanarayanan & Slaughter, 2006), we did not observe Ca^{2+} waves in response to depolarizing steps of 200 ms or longer, even when we used OGB-1, a high-affinity indicator (data not shown). This is consistent with other observations suggesting little role for Ca^{2+}-induced Ca^{2+} release in cones (Krizaj et al., 2003).

We next examined changes in Ca^{2+} evoked by depolarization to −35 mV, equivalent to the dark potential of cones. Only a small fraction of the voltage-gated Ca^{2+} conductance should be active at −35 mV (Thoreson et al., 2003). Nevertheless, steps to −35 mV elicited a clear increase in fluorescence (Fig. 2B), with Ca^{2+} hot spots reaching levels of several micromolars ($4.6 \pm 1.5\ \mu M$; $N = 4$). Thus, while Ca^{2+} levels in the terminal cytoplasm average ~360 nM in darkness, local Ca^{2+} levels near the channels are much higher.

We tested whether the sites of Ca^{2+} influx revealed with these dyes are close to the ribbon, as predicted by immunohistochemistry (Nachman-Clewner et al., 1999; Morgans, 2001; tom Dieck et al., 2005). To label synaptic ribbons, we used a *Rh*odamine-tagged *r*ibbon-*b*inding *p*eptide (Rh-RBP) that specifically binds to the ribbon protein ribeye (Zenisek et al., 2004). Rh-RBP and the Ca^{2+}-sensitive dye, OGB-6F, were introduced into cones through patch pipettes. Depolarization of the cone elicited a rise in OGB-6F fluorescence, indicating a localized rise in Ca^{2+}. The regions exhibiting the largest change in Ca^{2+} are again highlighted by subtracting the −70 mV image (Fig. 3A) from the −10 mV image (Fig. 3B). The resulting difference image shows three hot spots of Ca^{2+} (Fig. 3C). Consistent with the results using OGB-5N (Fig. 2), Ca^{2+} levels measured with OGB-6F in the hot spot rose to micromolar levels (Fig. 3D). Visualization of Rh-RBP in the same cell showed selective labeling of three spots at the base of the cone (Fig. 3E), where synaptic ribbons are located. Merging the OGB-6F and Rh-RBP images shows that the Ca^{2+} hot spots overlap with the ribbon labeling (Fig. 3F). Similar co-localization was seen in 11 photoreceptors (six rods and five cones). This suggests that high levels of Ca^{2+} are attained at the ribbon, the principle site of synaptic vesicle exocytosis.

It has been reported that the Ca^{2+} indicator dye Fluo-3 can accumulate on ribbons in hair cell terminals (Issa & Hudspeth, 1996), which could confound identification of local regions having a high Ca^{2+} concentration. However, OGB-6F fluorescence is weak at the hot spot region when the cell is hyperpolarized (Fig. 3A), indicating no local accumulation of the dye. Moreover, elevating Ca^{2+} homogenously by flash photolysis of caged Ca^{2+} (DM-nitrophen) did not produce hot spots (data not shown).

Discussion

Optical measurement of Ca^{2+} in light and darkness

The signaling steps that link photoreceptor light responses to suppression of neurotransmitter release have been studied chiefly with electrophysiological techniques. Thus, light-induced hyperpolarization (Baylor & Fuortes, 1970), the consequent decrease in voltage-gated Ca^{2+} current (Corey et al., 1984), and the resulting change in membrane capacitance resulting from Ca^{2+}-dependent exocytosis (Rieke & Schwartz, 1996; Thoreson et al., 2004) were all revealed by electrical recording methods. Only recently has optical imaging been applied to measuring the decrease in synaptic vesicle exocytosis in response to light (Choi et al., 2005a). Here, we used optical methods to visualize the one crucial signaling step between phototransduction and synaptic release that has remained unmeasured, the light-triggered decrease in synaptic Ca^{2+} concentration.

There are several technical challenges in optically measuring synaptic Ca^{2+} while keeping cones dark-adapted. The first challenge is minimizing the inadvertent photoisomerization of cone opsins while eliciting fluorescence from Ca^{2+} indicator dyes. Our solution is to use two-photon microscopy, which excites the dyes with long-wavelength light (>700 nm), largely outside the spectral range of photoreceptor activation. Even so, we are limited to capturing brief and infrequent "snapshots" of Ca^{2+}, as more prolonged or repeated (>5 s) illumination with these wavelengths does indeed elicit a photoresponse of sufficient magnitude to alter synaptic function (Sheng et al., 2007).

A second challenge is localizing Ca^{2+} signals with high spatial accuracy. Given our illumination parameters, diffraction limits direct microscopic resolution to ~300 nm (Stelzer, 2000). This blurring of the observed Ca^{2+} gradient limits the ability to accurately measure highly localized Ca^{2+} changes, leading to underestimation of their values (Augustine et al., 2003). Nevertheless, our measurements indicate that at a minimum, steady-state levels of Ca^{2+} at the base of the synaptic ribbon reach several micromolars in darkness. We expect that the local Ca^{2+} concentration probably reaches much higher levels at release sites, which appear to be located within nanometers of Ca^{2+} channels.

Roles of Ca^{2+} in synaptic transmission

In neurons that fire action potentials, voltage-gated Ca^{2+} channels are tightly localized near sites of synaptic vesicle fusion. This co-localization enables the high Ca^{2+} concentration in nanodomains near the mouth of an open channel (>100 μM) to saturate the release machinery on neighboring primed vesicles (Augustine et al., 2003; Schneggenburger & Neher, 2005). This arrangement ensures rapid and reliable phasic release of vesicles to a very brief stimulus, namely the action potential.

Photoreceptors, in contrast, generate graded voltage signals and release neurotransmitter in a tonic manner. Photoreceptor synapses have several biochemical and morphological specializations not found in conventional synapses, but how these specializations contribute to tonic release is not well understood. The Ca^{2+} sensor for neurotransmitter release in rods and cones has an unusually high affinity, enabling release at submicromolar Ca^{2+} levels (Rieke & Schwartz, 1996; Thoreson et al., 2004; Sheng et al., 2007). This would seem to alleviate the need for high local Ca^{2+} and therefore close association between Ca^{2+} channels and Ca^{2+}-sensitive release sites. In fact, it has been suggested that the sensor for neurotransmitter release is so far removed from Ca^{2+} channels so that vesicle fusion events are not tightly coordinated with individual channel opening events (Rieke & Schwartz, 1996). The present results revealed a twofold change in intraterminal Ca^{2+} levels between light and dark. A twofold change in Ca^{2+} levels should produce only a twofold change in synaptic release from cones (Thoreson et al., 2004; Sheng et al., 2007), but release rates vary 25-fold between light and dark (Choi et al., 2005a). These results therefore suggest that larger, local Ca^{2+} changes are more directly responsible for regulating release than average intraterminal Ca^{2+} levels.

We found that Ca^{2+} influx through voltage-gated Ca^{2+} channels in cones produced hot spots that tightly co-localize with synaptic ribbons, similar to results obtained in hair cells and retinal bipolar cells (Issa & Hudspeth, 1996; Zenisek et al., 2003, 2004). Furthermore, our results showed that micromolar dark Ca^{2+} concentrations are achieved near the base of ribbons and probably much higher concentrations near individual open Ca^{2+} channels. Our functional imaging results are also consistent with morphological evidence for Ca^{2+} channel localization near ribbons. Freeze-fracture Electron Microscopy studies show rows of intramembranous particles, proposed to be Ca^{2+} channels, at the base of synaptic ribbons (Raviola & Gilula, 1975), and more recent immuno-EM studies show labeling for α1 Ca^{2+} channel subunits clustered near synaptic ribbons (Nachman-Clewner et al., 1999; Morgans, 2001; tom Dieck et al., 2005).

Our measurements indicate that the average Ca^{2+} concentration at hot spots in darkness is at least 4 μM and likely to be much higher within 50 nm of voltage-gated Ca^{2+} channels. Studies using paired recordings from cones and bipolar cells show that depolarization to the dark potential of cones triggers a rapid burst of exocytosis with an instantaneous vesicle fusion rate of several thousand vesicles per second (DeVries & Schwartz, 1999; Rabl et al., 2005). However, measurements of FM1-43 release indicate that cones sustain a tonic release rate of only 250 vesicles per second in darkness (Choi et al., 2005a). This discrepancy between abrupt and tonic release rates would be predicted if release sites were quite distant from Ca^{2+} channels. However, our results show that Ca^{2+} channels are clustered close to the synaptic ribbon and average intraterminal Ca^{2+} changes are too small to account for light–dark changes in release rates. A more likely explanation is that the cone terminal is in a continual state of synaptic depression in darkness. The high release rates stimulated by membrane depolarization cannot be maintained for more than a few milliseconds because release sites are rapidly depleted of vesicles (Rabl et al., 2006). Thus, release from cones declines to slower tonic rates as they remain depolarized in darkness, despite the presence of locally high Ca^{2+} levels at the ribbon synapse.

Acknowledgments

We thank Katalin Rabl for help with salamander imaging experiments, David Zenisek for providing Rh-RBP, and Robert S. Zucker for helpful discussions. This work was supported by National Institutes of Health grants EY15514 to R.H.K. and EY10542 to W.B.T. and a sabbatical research grant to W.B.T. from Research to Prevent Blindness.

References

Augustine GJ, Santamaria F, Tanaka K. Local calcium signaling in neurons. Neuron 2003;40:331–346. [PubMed: 14556712]

Baldridge WH, Kurennyi DE, Barnes S. Calcium-sensitive calcium influx in photoreceptor inner segments. J Neurophysiol 1998;79:3012–3018. [PubMed: 9636104]

Baylor DA, Fuortes MG. Electrical responses of single cones in the retina of the turtle. J Physiol 1970;207:77–92. [PubMed: 4100807]

Cadetti L, Bryson EJ, Ciccone CA, Rabl K, Thoreson WB. Calcium-induced calcium release in rod photoreceptor terminals boosts synaptic transmission during maintained depolarization. Eur J Neurosci 2006;23:2983–2990. [PubMed: 16819987]

Cervetto L, Piccolino M. Synaptic transmission between photoreceptors and horizontal cells in the turtle retina. Science 1974;183:417–419. [PubMed: 4358073]

Choi SY, Borghuis BG, Rea R, Levitan ES, Sterling P, Kramer RH. Encoding light intensity by the cone photoreceptor synapse. Neuron 2005a;48:555–562. [PubMed: 16301173]

Choi SY, Sheng Z, Kramer RH. Imaging light-modulated release of synaptic vesicles in the intact retina: Retinal physiology at the dawn of the post-electrode era. Vision Res 2005b;45:3487–3495. [PubMed: 16185743]

Corey DP, Dubinsky JM, Schwartz EA. The calcium current in inner segments of rods from the salamander (Ambystoma tigrinum) retina. J Physiol 1984;354:557–575. [PubMed: 6090654]

Demuro A, Parker I. Imaging single-channel calcium microdomains. Cell Calcium 2006;40:413–422. [PubMed: 17067668]

DeVries SH, Schwartz EA. Kainate receptors mediate synaptic transmission between cones and 'Off' bipolar cells in a mammalian retina. Nature 1999;397:157–160. [PubMed: 9923677]

Fesenko EE, Kolesnikov SS, Lyubarsky AL. Induction by cyclic GMP of cationic conductance in plasma membrane of retinal rod outer segment. Nature 1985;313:310–313. [PubMed: 2578616]

Grynkiewicz G, Poenie M, Tsien RY. A new generation of Ca2+ indicators with greatly improved fluorescence properties. J Biol Chem 1985;260:3440–3450. [PubMed: 3838314]

Heidelberger R, Thoreson WB, Witkovsky P. Synaptic transmission at retinal ribbon synapses. Prog Retin Eye Res 2005;24:682–720. [PubMed: 16027025]

Helmchen, F. Calibration of fluorescent calcium indicators. In: Yuste, R.; Lanni, F.; Konnerth, A., editors. Imaging Neurons: A Laboratory Manual. Vol. chap 32. New York: Cold Spring Harbor Laboratory Press; 2000. p. 1-32.

Issa NP, Hudspeth AJ. Characterization of fluo-3 labeling of dense bodies at the hair cell's presynaptic active zone. J Neurocytol 1996;25:257–266. [PubMed: 8793731]

Johnson JE Jr, Perkins GA, Giddabasappa A, Chaney S, Xiao W, White AD, Brown JM, Waggoner J, Ellisman MH, Fox DA. Spatiotemporal regulation of ATP and Ca2+ dynamics in vertebrate rod and cone ribbon synapses. Mol Vis 2007;13:887–919. [PubMed: 17653034]

Krizaj D, Bao JX, Schmitz Y, Witkovsky P, Copenhagen DR. Caffeine-sensitive calcium stores regulate synaptic transmission from retinal rod photoreceptors. J Neurosci 1999;19:7249–7261. [PubMed: 10460231]

Krizaj D, Copenhagen DR. Compartmentalization of calcium extrusion mechanisms in the outer and inner segments of photoreceptors. Neuron 1998;21:249–256. [PubMed: 9697868]

Krizaj D, Lai FA, Copenhagen DR. Ryanodine stores and calcium regulation in the inner segments of salamander rods and cones. J Physiol 2003;547:761–774. [PubMed: 12562925]

Matthews G. Synaptic exocytosis and endocytosis: Capacitance measurements. Curr Opin Neurobiol 1996;6:358–364. [PubMed: 8794078]

Morgans CW. Localization of the δ1F calcium channel subunit in the rat retina. Invest Ophthalmol Vis Sci 2001;42:2414–2418. [PubMed: 11527958]

Morgans CW, El Far O, Berntson A, Wässle H, Taylor WR. Calcium extrusion from mammalian photoreceptor terminals. J Neurosci 1998;18:2467–2474. [PubMed: 9502807]

Nachman-Clewner M, St. Jules R, Townes-Anderson E. L-type calcium channels in the photoreceptor ribbon synapse: Localization and role in plasticity. J Comp Neurol 1999;415:1–16. [PubMed: 10540354]

Naraghi M, Neher E. Linearized buffered Ca2+ diffusion in microdomains and its implications for calculation of [Ca2+] at the mouth of a calcium channel. J Neurosci 1997;17:6961–6973. [PubMed: 9278532]

Prescott ED, Zenisek D. Recent progress towards understanding the synaptic ribbon. Curr Opin Neurobiol 2005;15:43143–43146.

Rabl K, Cadetti L, Thoreson WB. Kinetics of exocytosis is faster in cones than rods. J Neurosci 2005;25:4633–4640. [PubMed: 15872111]

Rabl K, Cadetti L, Thoreson WB. Paired-pulse depression at photoreceptor synapses. J Neurosci 2006;26:2555–2563. [PubMed: 16510733]

Raviola E, Gilula NB. Intramembrane organization of specialized contacts in the outer plexiform layer of the retina. J Cell Biol 1975;75:192–222. [PubMed: 1127010]

Rea R, Li J, Dharia A, Levitan ES, Sterling P, Kramer RH. Streamlined synaptic vesicle cycle in cone photoreceptor terminals. Neuron 2004;4:755–766. [PubMed: 15003175]

Rieke F, Schwartz E. Asynchronous transmitter release: Control of exocytosis and endocytosis at the salamander rod synapse. J Physiol 1996;493:1–8. [PubMed: 8735690]

Savchenko A, Barnes S, Kramer RH. Cyclic-nucleotide-gated channels mediate synaptic feedback by nitric oxide. Nature 1997;390:694–698. [PubMed: 9414163]

Schneggenburger R, Neher E. Presynaptic calcium and control of vesicle fusion. Curr Opin Neurobiol 2005;15:266–274. [PubMed: 15919191]

Sheng Z, Choi SY, Dharia A, Li J, Sterling P, Kramer RH. Synaptic Ca2+ in darkness is lower in rods than cones, causing slower tonic release of vesicles. J Neurosci 2007;27:5033–5042. [PubMed: 17494689]

Stelzer, EH. Practical limits to resolution in fluorescence light microscopy. In: Yuste, R.; Lanni, F.; Konnerth, A., editors. Imaging Neurons: A Laboratory Manual. New York: Cold Spring Harbor Laboratory Press; 2000. p. 12.1-12.9.

Suryanarayanan A, Slaughter MM. Synaptic transmission mediated by internal calcium stores in rod photoreceptors. J Neurosci 2006;26:1759–1766. [PubMed: 16467524]

Thoreson WB, Rabl K, Townes-Anderson E, Heidelberger R. A highly Ca^{2+}-sensitive pool of vesicles contributes to linearity at the rod photoreceptor ribbon synapse. Neuron 2004;42:595–605. [PubMed: 15157421]

Thoreson WB, Tranchina D, Witkovsky P. Kinetics of synaptic transfer from rods and cones to horizontal cells in the salamander retina. Neuroscience 2003;122:785–798. [PubMed: 14622921]

Tom Dieck S, Altrock WD, Kessels MM, Qualmann B, Regus H, Brauner D, Fejtova A, Bracko O, Gundelfinger ED, Brandstätter JH. Molecular dissection of the photoreceptor ribbon synapse: Physical interaction of Bassoon and RIBEYE is essential for the assembly of the ribbon complex. J Cell Biol 2005;168:825–836. [PubMed: 15728193]

Wilkinson MF, Barnes S. The dihydropyridine-sensitive calcium channel subtype in cone photoreceptors. J Gen Physiol 1996;197:621–630. [PubMed: 8740375]

Zenisek D, Davila V, Wan L, Almers W. Imaging calcium entry sites and ribbon structures in two presynaptic cells. J Neurosci 2003;23:2538–2548. [PubMed: 12684438]

Zenisek D, Horst NK, Merrifield C, Sterling P, Matthews G. Visualizing synaptic ribbons in the living cell. J Neurosci 2004;24:9752–9759. [PubMed: 15525760]

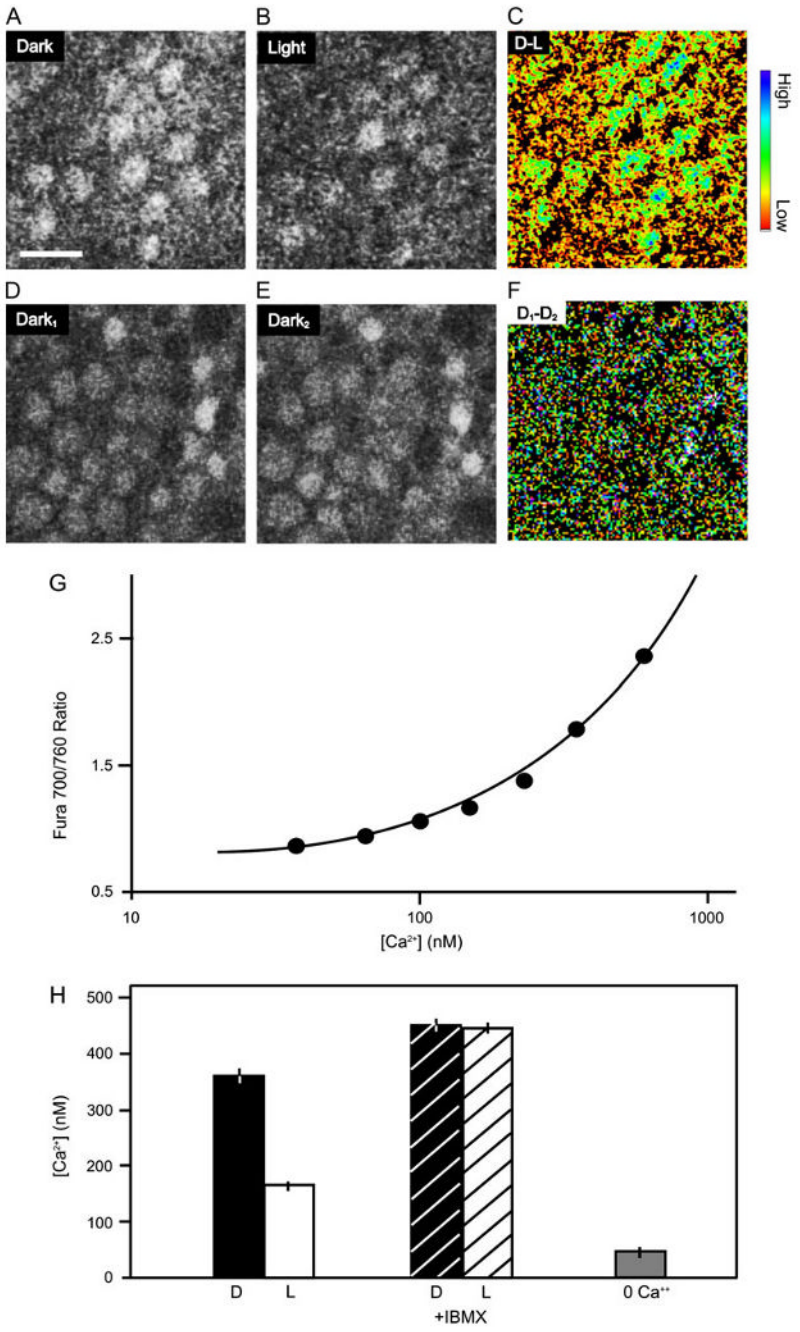

Fig. 1.

Light-elicited decrease in average Ca^{2+} in cone terminals. (**A-D**) Images from two-photon scans of OPL of a flat-mounted anole retina loaded with the Ca^{2+} dye OGB-1. To reveal the decrease in Ca^{2+} resulting from light, scans were taken from dark-adapted retina before (**A**) and after (**B**) 5-min illumination with white light. Pseudocolor difference image (scan in **B** − scan in **A**) highlights the drop in Ca^{2+} resulting from illumination (**C**) Scale bar in **A** is 10 μm. The blue end of the color scale represents a larger decrease in Ca^{2+}; the red end of the scale represents a smaller decrease. To control for possible effects of scanning, control scans were taken before (**D**) and after (**E**) a continued period of 5 min in darkness. The difference image (scan in **E** − scan in **D**) shows no decrease in Ca^{2+} (**F**). Quantification of spatially

averaged Ca^{2+} in cone terminals by two-photon imaging of fura-2. (**G**) The calibration curve was determined with a fura-2 calcium imaging calibration kit (Invitrogen) and fit with the standard equation (Grynkiewicz et al., 1985), yielding a best-fit K_d of 234 nM. For clarity, only the lower concentration portion of the sigmoidal calibration curve is shown (continuous line). (**H**) White light stimulation causes a 50% drop in internal Ca^{2+}. Blocking rod and cone PDE with IBMX leads to a rise in Ca^{2+} above the dark level and eliminates the effect of light. Exposing the retina to Ca^{2+}-free saline for 15 min causes Ca^{2+} to drop below the light level.

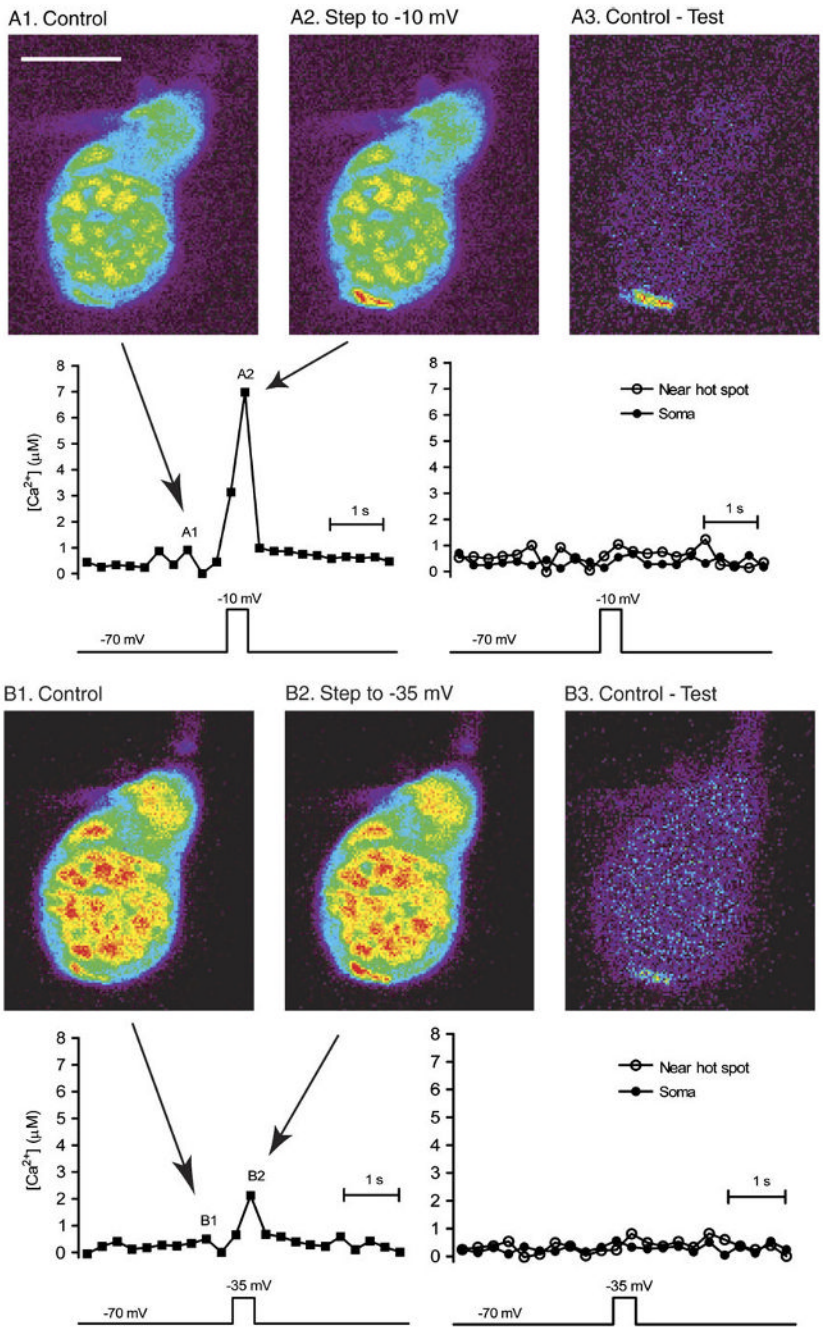

Fig. 2.

Depolarizing steps to −35 and −10 mV evokes localized Ca^{2+} increases in voltage-clamped cones that can be detected with the low-affinity Ca^{2+} dye, OGB-5N. The figure shows pseudocolor images from a single confocal section of a cone filled with OGB-5N. **A1** is a control image obtained prior to the depolarizing test step. **A2** shows the image obtained during the last 55 ms of a 200-ms depolarizing test step from −70 to −10 mV, which produced a localized fluorescence increase in the synaptic region at the base of the cone. The Ca^{2+} hot spot can be seen more clearly in the difference image in **A3**. The graphs show changes in Ca^{2+} over time for regions within the hot spot (left graph), just to the upper right of the hot spot (right graph), and in the soma (right graph). $\Delta F/F$ was converted to $[Ca^{2+}]$ using eqn (1).

Images illustrated in the figure were acquired at time points indicated in the left graph. **B1** shows a subsequent control image obtained in the same cone, **B2** shows an image of the cone obtained during a depolarizing step from −70 to −35 mV, and **B3** shows the difference image of the hot spot produced by this modest depolarization. OGB-5N was imaged with 488-nm excitation and 525-nm emission filters. As in panel **A**, the graphs show $[Ca^{2+}]$ as a function of time for the hot spot, an adjacent region, and the soma. Image acquisition time: 55 ms. Scale bar = 10 μm.

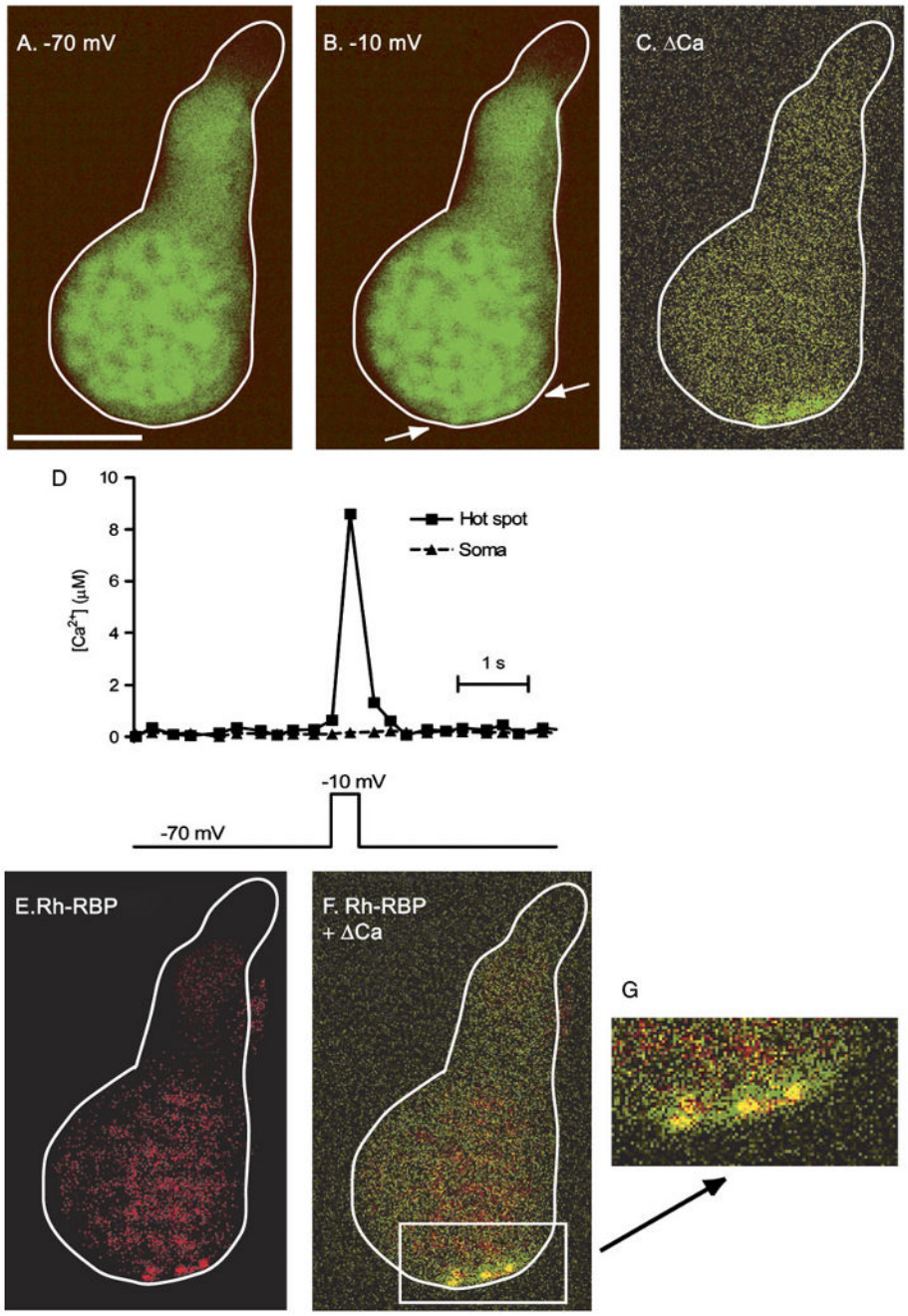

Fig. 3.

Ca^{2+} hot spots co-localize with synaptic ribbons. Cone loaded via a patch pipette with the low-affinity Ca^{2+} indicator dye OGB-6F and the ribbon-specific peptide, Rh-RBP. Fluorescent images were taken at −70 mV (**A**) and during depolarization to −10 mV (**B**). The voltage clamp stimulus and times at which images **A** and **B** were obtained are illustrated below the images. Difference image (**C**) shows regions at the base of the terminal exhibiting increased fluorescence (green pixels), indicating a higher Ca^{2+} concentration. Note the three Ca^{2+} "hot spots." OGB-6F was imaged with 488-nm excitation and 525-nm emission filters. Duration of each frame during Ca^{2+} imaging was 48 ms. (**D**) The graph shows changes in Ca^{2+} within the hot spot and soma over time. $\Delta F/F$ was converted to $[Ca^{2+}]$ using eqn (1) and a K_d of 3 μM

for OGB-6F. (**E**) Binding of Rh-RBP to synaptic ribbons in the same cone was visualized by exciting the dye with 568-nm excitation and 607-nm emission filters. Note the three spots of bright labeling (red pixels), presumably from three distinct synaptic ribbons. (**F**) Overlap of the change in OGB-6F fluorescence and Rh-RBP binding (yellow pixels), showing co-localization of Ca^{2+} hot spots and synaptic ribbons (panel C + panel E). (**G**) Magnification of the region containing Ca^{2+} hot spots. Scale bar =10 μm.